Supporting Information

Acceleration of liquid-crystalline phase transition simulations using selectively scaled and returned molecular dynamics

Ryoma Sasaki[†,‡], Yoshihiro Hayashi, [a, c] Susumu Kawauchi [*,†,‡,¶]

[†]Department of Chemical Science and Engineering, School of Materials and Chemical Technology, Tokyo Institute of Technology, 2-12-1-E4-6 Ookayama, Meguro-ku, Tokyo 152-8552, Japan.
[‡]Tokyo Tech Academy for Convergence of Materials and Informatics (TAC-MI), Tokyo Institute of Technology, 2-12-1 Ookayama, Meguro-ku, Tokyo 152-8552, Japan.
[¶]Research Institute of Polymer Science and Technology (RIPST), Tokyo Institute of Technology, 2-12-1 Ookayama, Meguro-ku, Tokyo 152-8552, Japan.
*Corresponding author, E-mail: kawauchi.s.aa@m.titech.ac.jp

Table of Contents

Force field parameters and topology for 4-octyl-4'-cyanobiphenyl (8CB).....S2
Comparison between Charge_mono and Charge_di models (384-molecule system) S4
Simulated transition from the nematic to smectic A phase of the Charge_di model (2048-molecule system).....S8
Selectively scaled MD with extremely low scaling factor $\alpha_{\text{inter-alkyl}}$ = 0.01 .....S9
References S10

Force field parameters and topology for 4-octyl-4'-cyanobiphenyl (8CB)

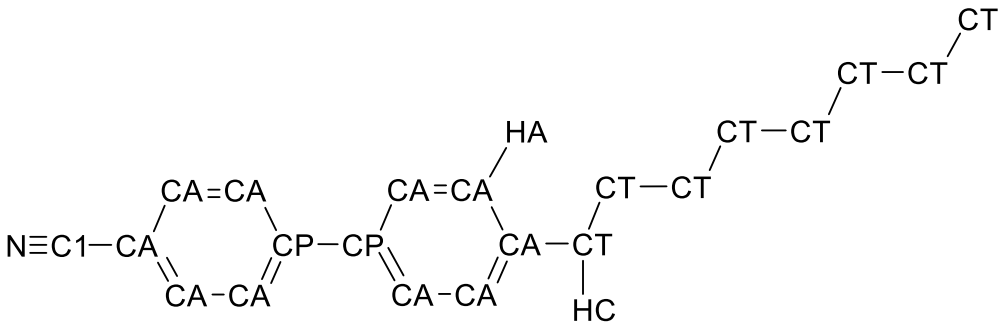

Figure S1. Atom types for 8CB.

Table S1. Lennard-Jones parameters.

Atom Type	ε (kcal·mol^{-1})	σ (Å)
CT	0.1094	3.331605
N1	0.17	3.184963
HA	0.015	2.547614
HC	0.0157	2.596613
CA	0.086	3.331605
C1	0.086	3.331605
CP	0.086	3.331605

Table S2. Bond-stretching parameters.

Bond type	K_b (kcal·mol^{-1}·Å^{-2})	r_0 (Å)
CA-CA	469	1.4
CA-HA	367	1.08
CA-CP	469	1.4
CP-CP	469	1.4
C1-CA	404.1	1.44
C1-N1	1014.5	1.138
CA-CT	317	1.51
CT-CT	310	1.526
CT-HC	340	1.09

Table S3. Bond-angle bending parameters.

Angle Type	K_a (kcal·mol^{-1}·degree^{-2})	$\boldsymbol{\theta}_0$ (°)
CA-CA-CA	63	120
CA-CA-HA	35	120
CA-CA-CP	63	120
CP-CA-HA	35	120
CA-CP-CA	63	120
CA-CP-CP	63	120
C1-CA-CA	65.9	120
CA-CA-CT	70	120
CA-CT-CT	63	114
CA-CT-HC	50	109.5
CT-CT-HC	50	109.5
HC-CT-HC	35	109.5
CT-CT-CT	40	109.5
CA-C1-N1	63	180

Table S4. Dihedral parameters.

Dihedral Type	K_a (kcal·mol^{-1})	δ (°)	n
X-CA-CA-X	3.625	-180	2
X-CA-CT-X	0	0	2
X-CT-CT-X	0.16	0	3
X-CA-CP-X	3.625	180	2
X-CP-CP-X	0.745	-180	2

Table S5. Improper parameters.

Improper Type	K_i (kcal·mol^{-1}·degree^{-2})	χ_0 (°)
HA-CA-X-X	1.1	0
X-CA-X-X	1.1	0
CT-CA-CA-CA	1.1	0

Comparison between Charge_mono and Charge_di models (384-molecule system)

In order to investigate the polarization effect of cyano groups on the property of liquid-crystalline phases, we examined the densities, orientational order parameter $\langle P_2 \rangle$, positional order parameter $\langle \tau_{CN} \rangle$, and phase transition temperatures (the experimental values[1]: smectic A–306.05 K–nematic–313.15 K–isotropic) using two models: the Charge_mono model and the Charge_di model, used to calculate the partial charges of the monomer and the dimer (**Figure** 2 in the main text), respectively. The *NpT* calculations started from the amorphous 384-molecule system at various temperatures. In general, simulation of the first-order phase transitions requires such a long simulation time that our calculations were run for 300–900 ns. The data in **Figures S2–S4** were obtained by averaging the last 100 ns trajectory. The temperature dependencies of the density and the order parameters ($\langle P_2 \rangle$ and $\langle \tau_{CN} \rangle$) are shown in **Figures S2** and **S4**, respectively. Similar to the previous MD studies of liquid crystals,[2–4] considering a system with $\langle P_2 \rangle > 0.4$ (Ref. 2–4) and $\langle \tau_{CN} \rangle < 0.1$ (Ref. 2) as the nematic phase, the predicted nematic–isotropic transition temperatures are 302.5 ± 2.5 K ($^{384\text{-mono}}T_{NI}$) and 322.5 ± 2.5 K ($^{384\text{-di}}T_{NI}$) for Charge_mono and Charge_di, respectively. In addition, the Charge_di model shows a sharp change of $\langle \tau_{CN} \rangle$ at 312.5 ± 2.5 K, which suggests the smectic A–nematic transition temperature ($^{384\text{-di}}T_{SmAN}$). In the Charge_mono model, a sharp change for $\langle \tau_{CN} \rangle$ was not obtained. It is noteworthy that the results of the smectic phase of the 384-molecule system include an uncertainty derived from the finite-size effect; this is because a smectic phase simulation

requires a >1000-molecule system as at least three layers are needed in the cell with a periodic boundary condition.

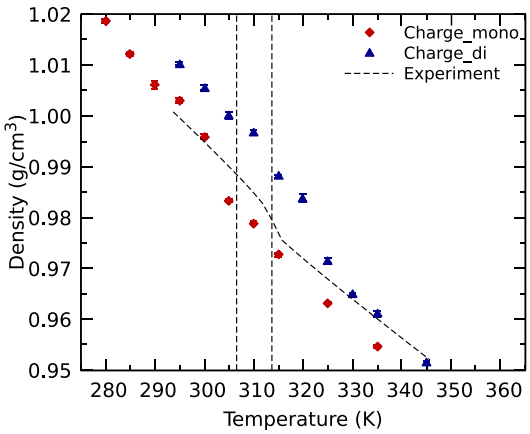

Figure S2. Simulated (Charge_mono and Charge_di models) and experimental (dashed red line) density of 8CB as a function of temperature. The dashed vertical lines indicate the experimental transition temperatures from nematic to smectic A and those from the isotropic to nematic phase.

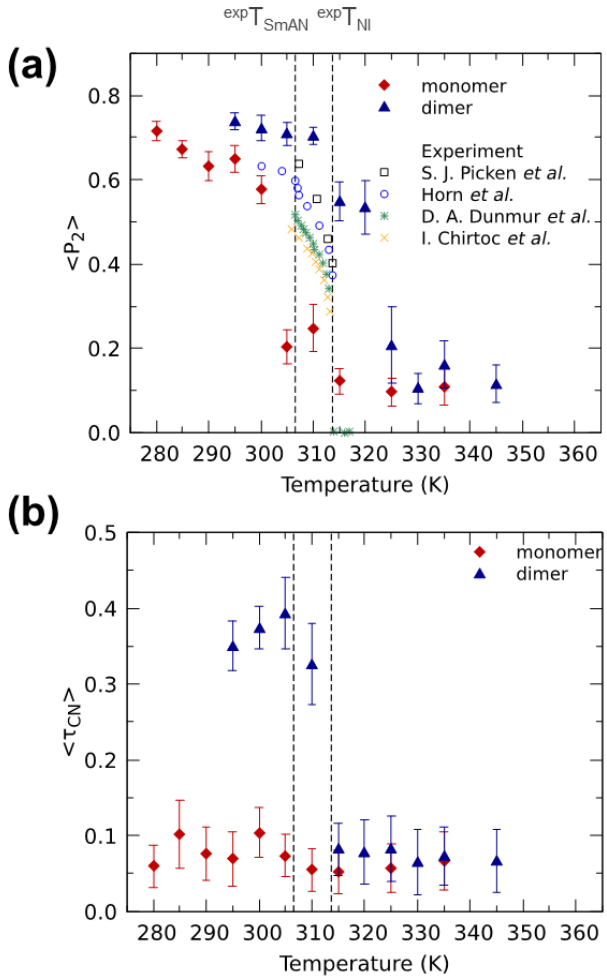

Figure S3. Simulations (Charge_mono and Charge_di models) of: (a) orientational order parameter $\langle P_2 \rangle$ with the experimental values (□[5], ○[6], *[7], ×[8]) and (b) $\langle \tau_{CN} \rangle$ as a function of temperature. The dashed vertical lines indicate the experimental transition temperatures from nematic to smectic A ($^{exp}T_{SmAN}$) and from isotropic to nematic phase ($^{exp}T_{NI}$), respectively.

Structural analyses were performed in the nematic phases at $^{384}T_{NI} - 2.5$ K to discuss the difference of the phase behavior between the Charge_mono and Charge_di models. The radial distribution function $g(r)$ and orientational correlation function $g_1(r) = \langle \cos\theta(r) \rangle$ of the cyano groups are shown in **Figure S4**. The first peak of $g(r)$ shown in **Figure S4**a and $g_1(r)$ shown in **Figure S4**b of the Charge_di model is stronger than that of the Charge_mono model, which means that the Charge_di

model is more likely to have an antiparallel dimer configuration due to the larger dipole moment considering polarization effect. Furthermore, this suggests that stabilization of the antiparallel dimer configuration due to the polarization effect of cyano groups contributes to the formation of the smectic phase of 8CB because the smectic A phase was obtained only in the Charge_di model (**Figure 5**b in the main text).

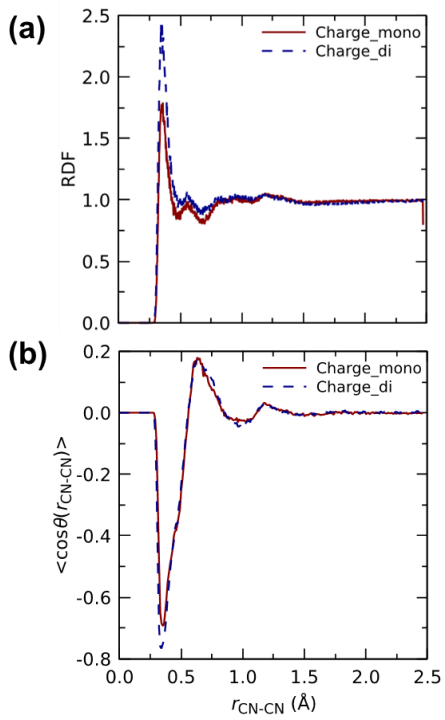

Figure S4. (a) Radial distribution function $g(r)$ and (b) orientational correlation function $g_1(r)$ of the cyano groups in the Charge_mono and Charge_di models.

Simulated transition from the nematic to smectic A phase of the Charge_di model (2048-molecule system)

The *NpT* calculation at 305 K was run from the nematic phase of the 2048-molecule system. According to the time evolution of P_2 and τ_{CN} (**Figure S5**b), P_2 continued above 0.4 and τ_{CN} increased to more than 0.3, demonstrating that the nematic phase changed to the smectic A phase. In addition, **Figure S5**a shows the formed smectic layer. Therefore, the phase transition from the nematic A to the smectic A phase occurred spontaneously.

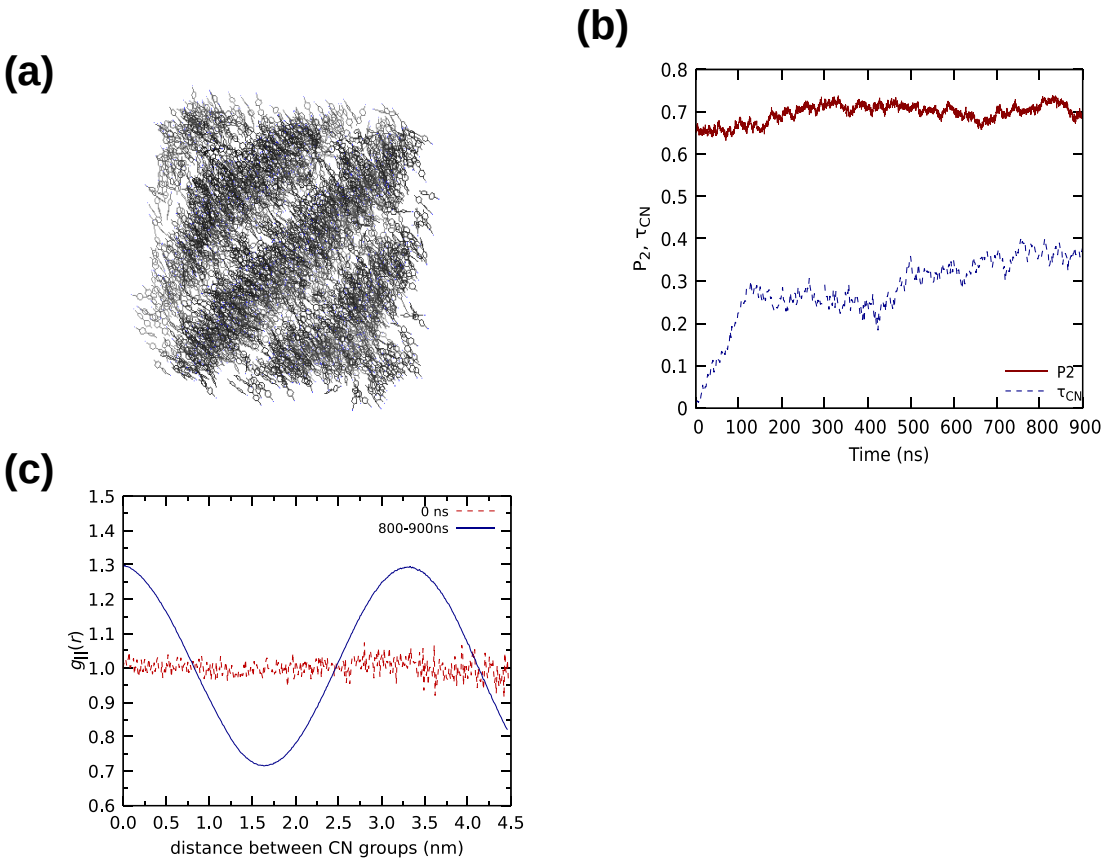

Figure S5. (a) Snapshot of the mesogenic group of the smectic A phase of 8CB (density = 999 kg·m^{-3} and Time = 900 ns) and (b) time evolution of P_2 and τ_{CN} of the 2048-molecule system (Charge_di model) from the nematic A phase to the smectic phase at 305 K.

Selectively scaled MD with extremely low scaling factor $\alpha_{\text{inter-alkyl}}$ = 0.01

A simulation at extremely small $\alpha_{\text{inter-alkyl}}$ (= 0.01) was performed; the obtained last snapshot is shown in **Figure S6**. This system has a twisted layer structure like that of cubic liquid crystals. The layers may have been twisted to relax the repulsion between the alkyl chain perpendicular to the mesogenic group. This result suggests ssrMD can be useful for modeling not only the smectic A phase, but also the cubic-like phase.

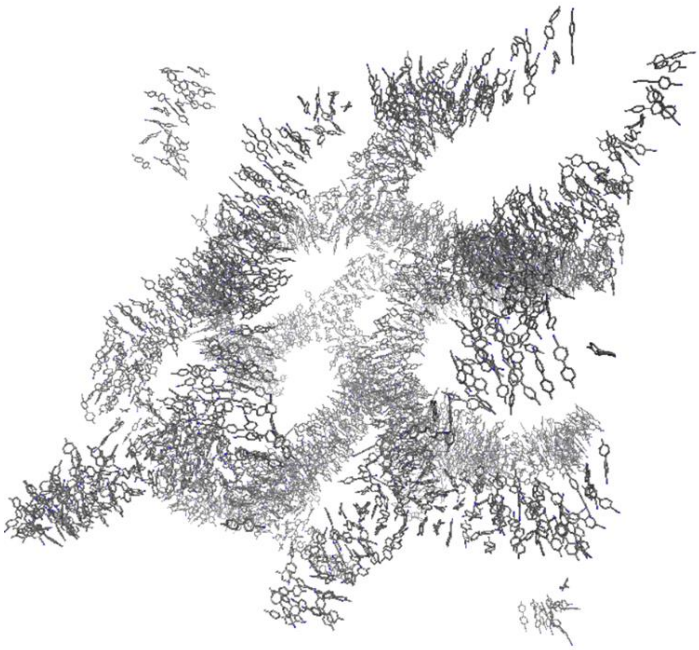

Figure S6. Snapshot of the mesogenic group obtained by ssMD with $\alpha_{\text{inter-alkyl}}$=0.01 (density = 278 kg·m^{-3}, P_2 = 0.14, and Time = 40 ns).

References

(1) Sandmann, M.; Würflinger, A. PVT Measurements on 4'-n-Octyl-Biphenyl-4-Carbonitrile (8CB) up to 300 MPa. *Z. Naturforsch* **1998**, *53a*, 787–792.

(2) Zhang, J.; Su, J.; Guo, H. An Atomistic Simulation for 4-Cyano-4'-Pentylbiphenyl and Its Homologue with a Reoptimized Force Field. *J. Phys. Chem. B* **2011**, *115*, 2214–2227.

(3) Wei, X.; Hooper, J. B.; Bedrov, D. Influence of Electrostatic Interactions on the Properties of Cyanobiphenyl Liquid Crystals Predicted from Atomistic Molecular Dynamics Simulations. *Liq. Cryst.* **2016**, *44*, 332–347.

(4) Boyd, N. J.; Wilson, M. R. Optimization of the GAFF Force Field to Describe Liquid Crystal Molecules: The Path to a Dramatic Improvement in Transition Temperature Predictions. *Phys. Chem. Chem. Phys.* **2015**, *17*, 24851–24865.

(5) Picken, S. J. Measurements and Values for Selected Order Parameters. In *Physical Properties of Liquid Crystals, Vol. 1: Nematics*; Dunmur, D. A., Fukuda, A., Luckhurst, G. R., Eds.; IEE: London, 2001; pp 89–102.

(6) Horn, R. G. Refractive Indices and Order Parameters of Two Liquid Crystals. *J. Phys. Fr.* **1978**, *39*, 105–109.

(7) *Physical Properties of Liquid Crystals, Vol. 1 : Nematics*; Dunmur, D. A., Fukuda, A., Luckhurst, G. R., Eds.; Institution of Electrical Engineers: London, 2001.

(8) Chirtoc, I.; Chirtoc, M.; Glorieux, C.; Thoen, J. Determination of the Order Parameter and Its Critical Exponent for nCB (n=5-8) Liquid Crystals from Refractive Index Data. *Liq. Cryst.* **2004**, *31*, 229–240.